Holographic data storage: optimized scheduling using the nonlocal polymerization-driven diffusion model

John T. Sheridan,* Feidhlim T. O'Neill, and John V. Kelly

Department of Electronic and Electrical Engineering, Faculty of Engineering and Architecture, University College Dublin, National University of Ireland, Belfield, Dublin D-4, Republic of Ireland

Received June 30, 2003; revised manuscript received January 15, 2004; accepted January 23, 2004

The choice of an exposure schedule that maximizes the uniformity and capacity of a holographic recording medium is of critical importance in ensuring the optimum performance of any potential holographic data storage scheme. We propose a methodology to identify an optimum exposure schedule for photopolymer materials governed by the nonlocal polymerization-driven diffusion model. Using this model, the relationship between the material properties (nonlocality and nonlinearity), the recording conditions and the schedule are clarified. In this way, we provide a first-order comparison of the behavior of particular classes of photopolymer materials for use as holographic storage media. We demonstrate, using the nonlocal polymerization-driven diffusion model, that the exposure schedule is independent of the number of gratings to be recorded and that the optimum schedule may necessitate leaving unpolymerized monomer at the end of the recording process. © 2004 Optical Society of America

OCIS codes: 090.0090, 090.2900, 090.4220, 090.5640, 090.7330, 210.2860, 210.4810, 210.0210, 160.5470, 160.4890, 050.0050, 050.1950, 050.7330.

1. INTRODUCTION

Photopolymer materials require no chemical postprocessing, exhibit low loss, low scatter, and high diffraction efficiencies (large modulations), and are relatively inexpensive.[1,2] They therefore possess major advantages in the race to be the medium of choice for both write-once read-many holographic data storage[3–6] and for the fabrication of bulk and micro holographic optical elements.[7–9]

When using a photopolymer as a holographic data storage medium, one wishes to choose a recording (exposure) schedule that optimizes the total polymer generated as a direct result of the recording process and at the same time produces M gratings of maximum and ideally equal strength (refractive-index modulation size). Although work has been carried out to examine optimum scheduling experimentally and to compare multiplexing techniques,[5,10–12] the material mechanisms involved and their effects on scheduling have not been clarified. The need for highly repetitive experimental procedures is due to the fact that no model has been available that satisfactorily explains the main material response characteristics of photopolymer materials.

The nonlocal polymerization-driven diffusion model (NPDD) was introduced in an attempt to explain, in a single model, all the most significant experimentally observed results, including low and high spatial frequency cutoffs and reciprocity failure.[13–16] In the NPDD, although diffusion is important in the grating-formation process, high spatial frequency cutoff is explained by assuming that chains grow away from their point of initiation. This material model is in the process of development, and its full range of validity, especially when combined with rigorous electromagnetic models, is being explored.[17–20] However, the NPDD has allowed the quantitative comparison of different materials[15,16] and has provided insights into the behavior of photopolymer materials.[21]

The two-harmonic version of this model has a significant range of validity[14] and can be used to derive approximate analytic solutions. It has been used in conjunction with Kogelnik's first-order coupled-wave model[7] to characterize photopolymer materials.[14–16] Combined with rigorous electromagnetic methods, the NPDD has also been applied recently to examine commercial holographic materials for use in the fabrication of waveguide components.[8] In this paper, the two-harmonic NPDD is used to derive an optimum exposure schedule for a holographic storage medium. For the sake of brevity, we will not review all the physical assumptions used in the derivation of the NPDD.[13,14]

We summarize the problem as follows:

(a) We wish to produce M sinusoidal gratings in a single material layer of equal refractive-index modulation.

(b) We wish to optimize the total polymer generated, thus optimizing the modulation of each grating.

In order to solve this problem, we assume the following:

1. The NPDD (with a Gaussian response function[13]) is valid for some class of photopolymer materials. This assumption is supported by the model's agreement with experimental results, carried out with different recording materials.[8,15,16] More specifically, we assume that the approximate two-harmonic analytic solutions are valid.[14] In this paper, we validate these analytic expressions for low-exposure recordings.

2. The monomer concentration distribution equalizes, through diffusion, between exposures. In recent papers, it has been demonstrated that, despite the relatively slow diffusion processes that may take place in different materials:

(a) Staggered exposures followed by repeated relaxation periods can be used to overcome constraints placed on photopolymer materials due to reciprocity failure.[22]

(b) We have previously reported measurements[23] of the relaxation of a strongly exposed acrylamide-based material containing both uncrosslinked polymer and monomer distributions. We have shown that complete relaxation can require several minutes. In the analysis presented here, we place no constraint on the relaxation time necessary. Furthermore, we assume no variation of the diffusion constant as a function of exposure. We simply assume that sufficient time is allowed for full monomer relaxation to take place and that any change in the diffusion constant is equivalent to a change in the R parameter[13,14]; see Eq. (3). It must be noted that, in a commercial data storage system, allowing for long relaxation times between exposures may be impractical. It appears, however, that the analysis presented here might be modified, following the form of analysis presented in Ref. 23, to model a situation of partial/incomplete material relaxation between exposures.

3. Although ultimately diffraction efficiency defines output signal strength, we assume it can be controlled independent of grating formation by varying layer thickness. Therefore we assume that an ideal uniform volume grating is formed and we can ignore (i) grating nonuniformities, (ii) layer shrinking/swelling, (iii) induced surface-relief gratings, (iv) that, during each exposure, no previously recorded grating are replayed, and (v) that scatter by the material is negligible before and after recording.[7] In this case, by varying the grating thickness (layer depth), the diffraction efficiency and angular selectivity can be controlled. We note that commercially available storage media have been reported that exhibit extremely good behavior.[10]

Finally, we note that the analysis presented here is based on the storage of a highly idealized data pattern, i.e., exposure with a maximum fringe visibility, $V = 1$, sinusoidal interference pattern. The inclusion of a nonlinear material effect does, however, mean that, effectively, a spectrum of gratings, simultaneously recorded, is modeled. Our predictions for several combinations of material and recording parameters are presented, where the parameters used are of the same order of magnitude as those determined experimentally.[8,14] In this way, we present a first-order study of the behavior of particular classes of photopolymer materials for use as holographic storage media.

2. THEORETICAL ANALYSIS: MATERIAL CHARACTERISTICS

Assume a sinusoidal interference pattern of amplitude I_0, period Λ, and fringe visibility $V = 1$ is used for the ith exposure, of duration t_i, of a holographic material with an initially uniform monomer concentration, $u_0^{(i)}(0)$. Since the initial monomer distribution is uniform, all higher monomer harmonics are assumed negligible, i.e., $u_1^{(i)}(0) = 0$. In the two-harmonic NPDD approximation,[14–16] the analytic solution found for the average, or zero-order harmonic, of monomer concentration is of the form

$$u_0^{(i)}(\xi_i) = u_0^{(i)}(0) \times \bar{u}_0(\xi_i), \tag{1a}$$

where $\xi_i = F_0 t_i = \kappa I_0^{\gamma} t_i$,[13,14] which is related to the ith exposure energy, $E_i = I_0 t_i$, κ is a constant, and where we previously derived the dimensionless factor,[15]

$$\bar{u}_0(\xi_i) = \exp\left[-(W + f_0)\frac{\xi_i}{2}\right]\left[\cosh\left(B\frac{\xi_i}{2}\right) + \left(\frac{W - f_0}{B}\right)\sinh\left(B\frac{\xi_i}{2}\right)\right]. \tag{1b}$$

For the sake of brevity, we have introduced the parameters $W = S(f_0 + f_2/2) + R$ and $B = [(W - f_0)^2 + 2f_1^2 S]^{1/2}$, where

$$S = \exp(-K^2\sigma/2), \tag{2}$$

$$R = DK^2/F_0 = R_0/(I_0^{\gamma}\Lambda^2). \tag{3}$$

σ quantifies the effects of nonlocal polymerization due to chain growth (propagation) away from the point of initialization.[13] $K = 2\pi/\Lambda$ is the grating vector magnitude. D is the diffusion constant of the monomer inside the material, which is assumed not to change during exposure, and therefore $\alpha = 0$.[13] F_0, the rate of polymerization, has been assumed to be either a linear function of the illumination intensity I_0 or a function of the illumination intensity I_0 raised to the power $\gamma = 1/2$.[14,15] The parameters (f_0, f_1, f_2) are Fourier coefficients introduced to take account of γ.[14] We assume F_0 does not vary as a function of time.

The corresponding expression for the first-harmonic polymer concentration is

$$N_1^{(i)}(\xi_i) = u_0^{(i)}(0) \times \bar{N}_1(\xi_i). \tag{4a}$$

Once again, we emphasize the dependence on the initial concentration of monomer and define the dimensionless function,[15]

$$\bar{N}_1(\xi_i) = \frac{4f_1 S}{(W + f_0)^2 - B^2}\left\{R + \exp\left[-\frac{(W + f_0)\xi_i}{2}\right] \times \left[\left(\frac{L}{B}\right)\sinh\left(\frac{B\xi_i}{2}\right) - R\cosh\left(\frac{B\xi_i}{2}\right)\right]\right\}, \tag{4b}$$

$L = (f_0 - R)R + [-f_1^2 + (f_0 + f_2/2)(2f_0 - R)]S$.

We assume the first-harmonic amplitude of the grating refractive-index modulation is linearly proportional to this polymer concentration.[13–16]

In order to observe the general characteristics of materials governed by these equations, we first present a set of four growth curves, Figs. 1(a) and 1(b) and Figs. 2(a) and 2(b). These show the variation of N_1 as a function of ξ, for a representative range of material (D, σ, α, γ, κ) and exposure (I_0, t, Λ, V) parameters. In each figure, two curves are shown, for the cases (i) $R = 10$ and (ii) $R = 0.1$. From the definition of R given in Eq. (3), we see

that each of these growth curves can be produced in several different physical situations. For example, keeping the spatial frequency (grating period) and exposing intensity constant, we could set (i) $D = 10F_0 \Rightarrow R = 10$ and then set (ii) $D = F_0/10 \Rightarrow R = 0.1$. However, situations having exactly the same R values occur for completely different recording situations. For example, keeping the material parameters D and κ constant, and (i) choosing an initial $I_0^{\gamma}\Lambda^2$ value for which $R = 10$, we could then set (ii) $I_0^{\gamma}\Lambda^2$ to a different value 100 times larger, giving $R = 0.1$. We further note that R can be maintained at a constant value even if the exposing period varies, since this can be compensated for by a variation of the exposing intensity, while the corresponding ξ values can remain unchanged by varying the exposure time t. In general, a material with a high R value would be expected to produce a high-fidelity recording, while as R decreases, higher-order grating harmonics will be generated, most noticeably during long exposures.[14,15]

From Figs. 1 and 2, we see that, as R increases, both the maximum value attained by N_1 increases and the value at which N_1 reaches its maximum value, ξ_M, increases. For $R = 10$, the maximum always occurs beyond the range of the figures, $\xi > 10$, while in all cases shown, when $R = 0.1$, a clear maximum always occurs for $\xi < 3$. This is significant when we later discuss data storage scheduling.

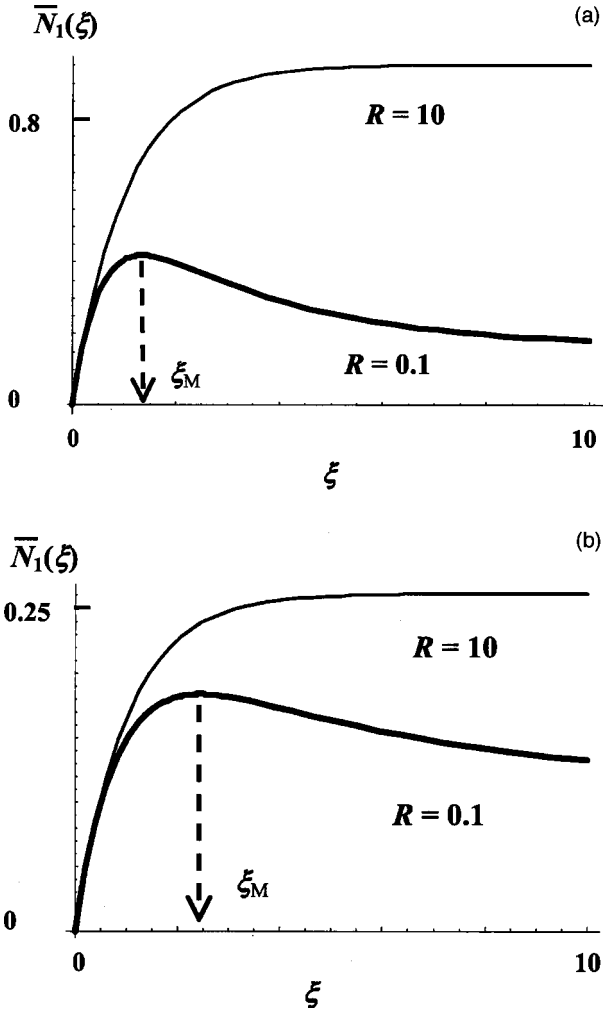

Fig. 1. (a) First harmonic of polymer-concentration growth curve, with $u_0^{(1)}(0) = 1$: $S = 1$ (local: $\sigma = 0$) and $\gamma = 1$ (linear). (b) First harmonic of polymer-concentration growth curve, with $u_0^{(1)}(0) = 1$: $S = 0.265$ (nonlocal: $\sigma/\Lambda^2 = 1/8$) and $\gamma = 1$ (linear).

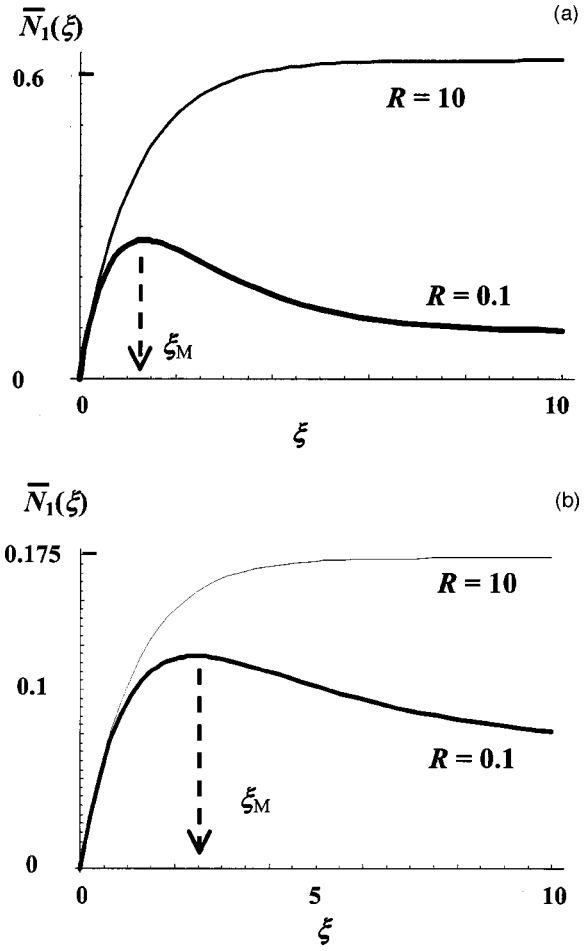

Fig. 2. (a) First harmonic of polymer-concentration growth curve, with $u_0^{(1)}(0) = 1$: $S = 1$ (local: $\sigma = 0$) and $\gamma = 1/2$ (nonlinear). (b) First harmonic of polymer-concentration growth curve, with $u_0^{(1)}(0) = 1$: $S = 0.265$ (nonlocal: $\sigma/\Lambda^2 = 1/8$) and $\gamma = 1/2$ (nonlinear).

The effects of varying S and γ are also explored in these figures. In Fig. 1(a) and Fig. 2(a), $S = 1$, and we assume the materials exhibit local reponses, $\sigma = 0$. In Fig. 1(b) and Fig. 2(b), the materials are assumed to exhibit significant nonlocal behavior with $S = 0.265$ and thus $\sigma/\Lambda^2 = 1/8$. Examining the figures, we note that, as S decreases (σ/Λ^2 increasing), the polymer-concentration growth curves decrease in size and the $R = 10$ and $R = 0.1$ curves become more similar in size. Furthermore, the smaller the value of S, the more slowly the material reaches its final steady-state value.

Finally, in Fig. 1, $\gamma = 1$, while in Fig. 2, $\gamma = 1/2$. We can therefore observe the effects of a nonlinear material response to the illuminating intensity. We note that the smaller the value of γ, the lower the N_1 growth curve maxima. Using the analytic expression and this range of γ values, γ is observed to have relatively little effect on the results.[17]

The validity of the analytic expressions, derived retaining only two harmonics, has previously been discussed in the case when it is assumed exposure continues until effectively all monomer present is polymerized,[14] i.e., when ξ is large. An indication of the range of validity and accuracy can be provided using the percentage difference between the four- and two-harmonic NPDD prediction of N_1,

$$\% \text{ error} = \frac{N_1(4\text{-harmonic}) - N_1(2\text{-harmonic})}{N_1(4\text{-harmonic})} \times 100. \tag{5}$$

It has previously been shown that, in all cases for which either $R > 1$ or $S < 0.25$, relatively good agreement, i.e., % error $< 10\%$, occurs for long exposures[14]; however, care must be taken to retain sufficient harmonics to ensure convergence for highly nonlinear and nonlocal materials.[8] No examination of the performance of the approximate analytic solutions, for the case when ξ is small, has previously been undertaken. We note that this case will be particularly important when many weak gratings are to be stored sequentially in a single medium. Therefore we compare the same material cases in Figs. 3 and 4 as were examined in Figs. 1 and 2. Following the procedure used previously,[14] we plot the percentage error in N_1 (% error), over the ranges $-2 < \log_{10}R < +2$ and $0.1 < S < 1$, when $\xi = 0.1$ and 1. Examining the results in Figs. 3 and 4, we note that, for the shorter exposures, the % error is at least an order of magnitude smaller than for the long-exposure case, $\xi > 10$, previously examined.[14] In keeping with the previous results, the errors are always smallest when $R > 1$ and $S < 0.25$. Significantly, we note that, as γ decreases, the % error increases by a factor of ~10, for shorter exposures.

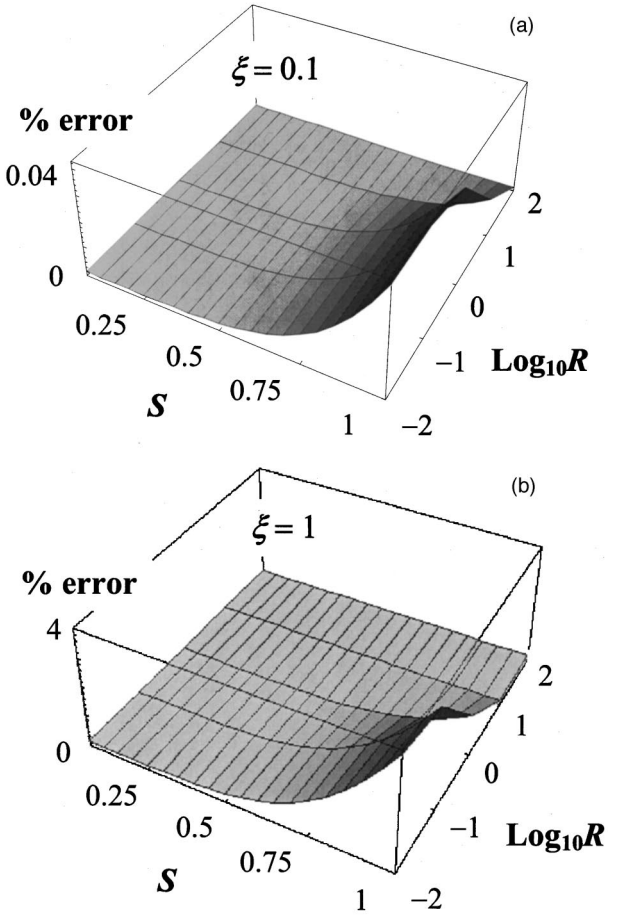

Fig. 3. (a) $\gamma = 1$ (linear). See Fig. 1(a). (b) $\gamma = 1$ (linear). See Fig. 1(b).

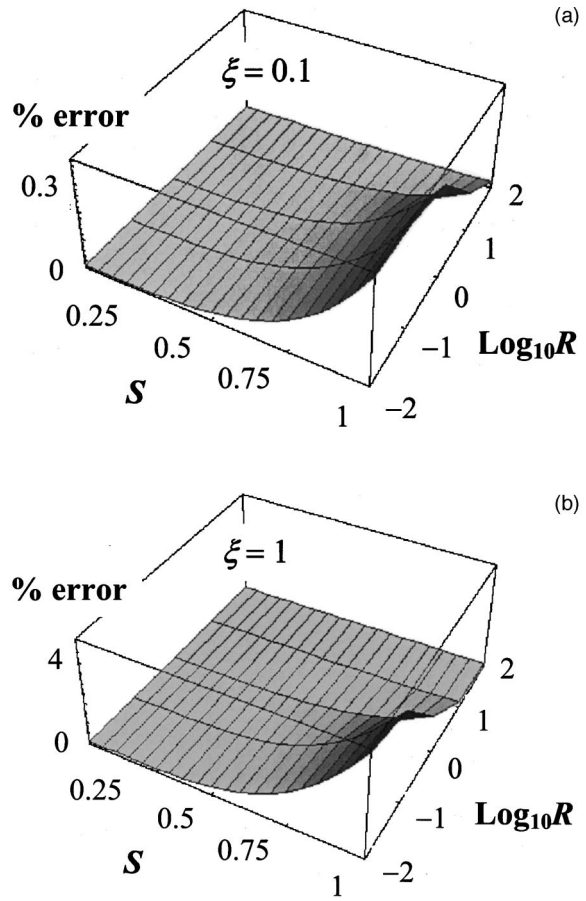

Fig. 4. (a) $\gamma = 1/2$ (nonlinear). See Fig. 2(a). (b) $\gamma = 1/2$ (nonlinear). See Fig. 2(b).

The most significant result of this analysis is that the analytic expressions are reasonably accurate over useful ranges of ξ, S, R and γ, and can therefore be used to estimate the holographic data storage schedule. We note that the results presented here reinforce and complement the detailed theoretical and experimental results presented elsewhere[13–20] and can be best appreciated in that fuller context.

3. THEORETICAL ANALYSIS: OPTIMUM DATA STORAGE SCHEDULE

As discussed in the introduction, we assume sufficient time is available between exposures to allow the monomer distribution to completely equalize through diffusion.[22,23] In this case, $u_0^{(i)}(\xi_i)$, the average monomer concentration at the end of the ith exposure, is the starting monomer concentration for the $(i+1)$th grating, and, in general, we can write that

$$u_0^{(i)}(\xi_i) = u_0^{(i-1)}(\xi_{i-1}) \times \bar{u}_0(\xi_i) = u_0^{(1)}(0) \times [\bar{u}_0(\xi_1) \times \bar{u}_0(\xi_2) \times \ldots \times \bar{u}_0(\xi_{i-1})] \times \bar{u}_0(\xi_i). \quad (6)$$

In previous papers,[13,14] it has been assumed that $u_0^{(1)}(0) = 100$, and we have then studied the case of a single continuous recording, $\xi = \xi_1$.

Similarly, for the ith exposure polymer concentration,

$$N_1^{(i)}(\xi_i) = u_0^{(i-1)}(\xi_{i-1})\bar{N}_1(\xi_i). \quad (7)$$

Therefore $N_1^{(i)}(\xi_i)$ depends on the monomer concentration left over after the previous recording. We require that all the gratings be equal; therefore

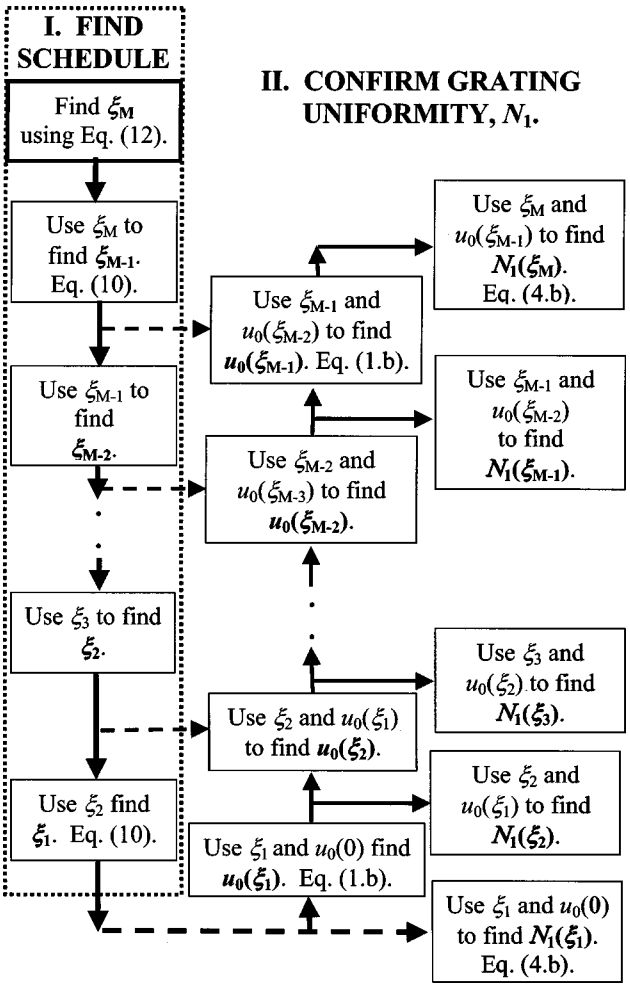

Fig. 5. Schedule optimization algorithm.

$$N_1^{(i)}(\xi_i) = N_1^{(i+1)}(\xi_i) \Rightarrow u_0^{(i-1)}(\xi_{i-1})\bar{N}_1(\xi_i) = u_0^{(i)}(\xi_i)\bar{N}_1(\xi_{i+1}). \quad (8)$$

After M recordings, the material contains the following total amount of polymer:

$$N_1^{\mathrm{TOT}} = \sum_{i=1}^{M} N_1^{(i)}(\xi_i) = u_0^{(1)}(0)\sum_{i=1}^{M}\left[\prod_{m=1}^{m=i-1}\bar{u}_0(\xi_m)\right]\bar{N}_1(\xi_i). \quad (9)$$

Since as much of the dynamic range as possible should be used, N_1^{TOT} must be maximized.

Combining Eqs. (6), (7), and (8), it can be shown that

$$\bar{N}_1(\xi_{i+1}) = \frac{\bar{N}_1(\xi_i)}{\bar{u}_0(\xi_i)}. \quad (10)$$

Given any suitable value of ξ_i, we can iteratively find all the ξ values that guarantee uniformity. For example, if an optimum value for the last exposure ξ_M is known, we can immediately find ξ_{M-1} by numerically solving the equation. Can an optimum ξ_M value be found? For the last exposure, $i = M$, the maximum possible grating that can be recorded for any initial monomer concentration will occur when

$$\left.\frac{\partial\bar{N}_1(\xi)}{\partial\xi}\right|_{\xi=\xi_M} = 0. \quad (11)$$

ξ_M can be found using any standard root-finding procedure. The ξ_M values for $R = 0.1$ are shown in Figs. 1 and 2. Choosing this value, we have automatically found the exposure, which maximizes the amplitude of the last grating. Substituting this value into Eq. (10), ξ_{M-1} can be found, and so on.

Once the complete set of ξ_i values is found for the M gratings, the associated polymer-concentration harmonic strength $N_1^{(i)}(\xi_i)$ can then be found by first substituting the ξ_{i-1} values back into the monomer formula, to give the initial monomer concentration for the ith exposure, $u_0(\xi_{i-1})$, and then calculating the polymer-concentration value. A flowchart representation of this scheduling procedure is given in Fig. 5.

Regarding the accuracy of our schedule results, we note that ξ_M is both the first and the largest ξ value to be estimated. The analytic expressions will therefore, in general, be most inaccurate in estimating it. Since an iterative technique is being used, any error introduced in this first value will affect the entire schedule, so ξ_M should ideally be found to a high degree of accuracy. This may necessitate the use of higher-order harmonic analysis or

Table 1. Exposures for Maximum N_1, % error = $100[\xi_M(4) - \xi_M(2)]/\xi_M(4)$

	$R = 0.1$; Linear, $\gamma = 1$			$R = 0.1$; Nonlinear, $\gamma = 1/2$		
$S(\sigma)$	Four-Harmonic $\xi_M(4)$	Two-Harmonic Analytic $\xi_M(2)$	% Error	Four-Harmonic $\xi_M(4)$	Two-Harmonic Analytic $\xi_M(2)$	% Error
Local: $S(0) = 1$	1.65	1.35	18%	1.48	1.34	9.5%
Nonlocal: $S = 0.265$	2.4	2.42	0.8%	2.41	2.42	0.4%

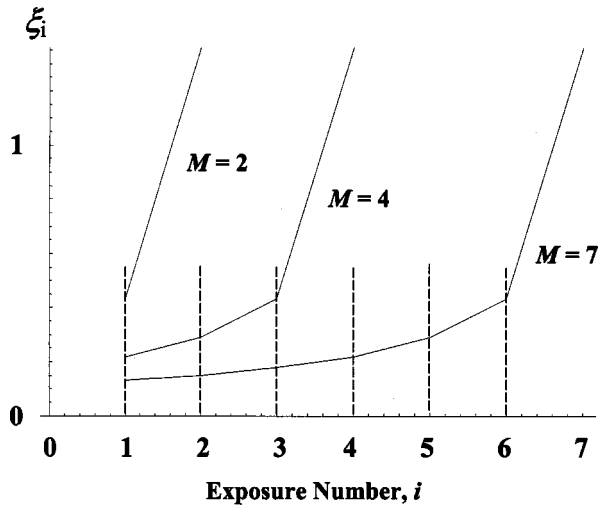

Fig. 6. ξ_i plotted as a function of i for different numbers of exposures M. $R = 0.1$, $\gamma = 1$ (linear), $S = 1$ (local case). Also see Tables 2 and 3.

Table 2. Schedules and Grating Strengths[a]

$R = 0.1$, $\gamma = 1$, $S = 1$ ($\sigma = 0$)				
i (M)	ξ_i	$N_1^{(i)}(\xi_i)$	$u_0^{(i)}(\xi_i)$	N_1^{TOT}
1	0.43	0.28	0.68	0.57
(**2**)	1.36		*0.25*	
1	0.29		0.76	
2	0.43	0.22	0.52	0.65
(**3**)	1.36		*0.20*	
1	0.22		0.81	
2	0.29	0.18	0.62	0.71
3	0.43		0.42	
(**4**)	1.36		*0.16*	
1	0.18		0.84	
2	0.22		0.69	
3	0.29	0.15	0.52	0.75
4	0.43		0.37	
(**5**)	1.36		*0.14*	

[a] $u_0(0) = 1$, $V = 1$, $\alpha = 0$. Also see Fig. 1(a).

direct solution of the partial differential equations.[8] In Table 1, the accuracy of the value of ξ_M calculated using the analytic function when $R = 0.1$ is tested. The ξ_M values obtained when retaining four or two harmonics, $\xi_M(4)$ and $\xi_M(2)$, and the percentage error between these values are tabulated for our four representative cases. As both S and γ decrease in size, corresponding to stronger nonlocal and nonlinear effects, the accuracy of the second-harmonic ξ_M estimate increases. In this paper, we assume these values are sufficiently accurate to provide a good first-order estimation of the optimum schedule.

4. HOLOGRAPHIC DATA STORAGE: RESULTS

We now present and discuss the optimum data storage schedules, which can be produced in the materials whose general characteristics have been examined in Figs. 1–4 above.

We first apply our algorithm to the case when $R = 0.1$, $\gamma = 1$ (linear: $f_0 = 1$, $f_1 = 1$, $f_2 = 0$), and $S = 1$ (local: $\sigma = 0$). We start by examining the behavior of the medium for low numbers ($M < 8$) of recorded gratings. The optimum schedules when $M = 2$, 4, and 7 are illustrated in Fig. 6, and a detailed set of predictions is presented in Table 2, for $M = 2$, 3, 4, and 5. Table 2 is organized as follows:

1. In the first column, we list the sequence of gratings, the bold numbers (in parentheses) indicating the total number of exposures.
2. In the second column, we give the values of ξ_i for each exposure. Examining the schedule, it is immediately clear that, for different values of M, the same ξ_i values reoccur.
3. In the third column are listed the first-harmonic polymer concentrations $N_1^{(q)}(\xi_q)$ in each grating (which are identical for uniform strength).
4. In the fourth column are listed the monomer concentrations remaining after each exposure. The values in italics in this column are the unused monomer concentrations left after the last exposure. We note that this quantity decreases as M increases.
5. The values in the last column, on the right-hand side, are the total polymer concentrations formed, $N_1^{\mathrm{TOT}} = M \times N_1^{(q)}(\xi_q)$. As can be seen, this value is much larger than the maximum value, which can be recorded in the single continuous exposure, shown for this case in Fig. 1(a). Furthermore, this total amount increases as the number of gratings stored increases.

We note that as M increases, the ratio ξ_M/ξ_1 increases dramatically. In practical storage systems, a large variation between the first and last exposures may be undesir-

Table 3. Corresponding to Fig. 1(a)

Local, $S = 1$; Linear, $\gamma = 1$ ($f_0 = 1, f_1 = 1, f_2 = 0$)				
	$R = 0.1$, $\xi_M = 1.3603$		$R = 10$, $\xi_M = 39.77$	
M	ξ_1	N_1	ξ_1	N_1
10	0.92545	0.0844	0.10608	0.0969
50	0.01952	0.0191	0.02012	0.01974
100	0.00986	0.0098	0.01002	0.0099
500	0.00199	0.0020	0.00200	0.0020
1000	0.00090	0.0010	0.00100	0.0010

Table 4. Corresponding to Fig. 1(b)

$\gamma = 1$ ($f_0 = 1, f_1 = 1, f_2 = 0$), $S = 0.265$, $R = 0.1$, $\xi_M = 2.4546$		
M	ξ_1	N_1
10	0.100610	0.025031
50	0.019980	0.005228
100	0.009990	0.002630
500	0.001999	0.000529
1000	0.000999	0.000265

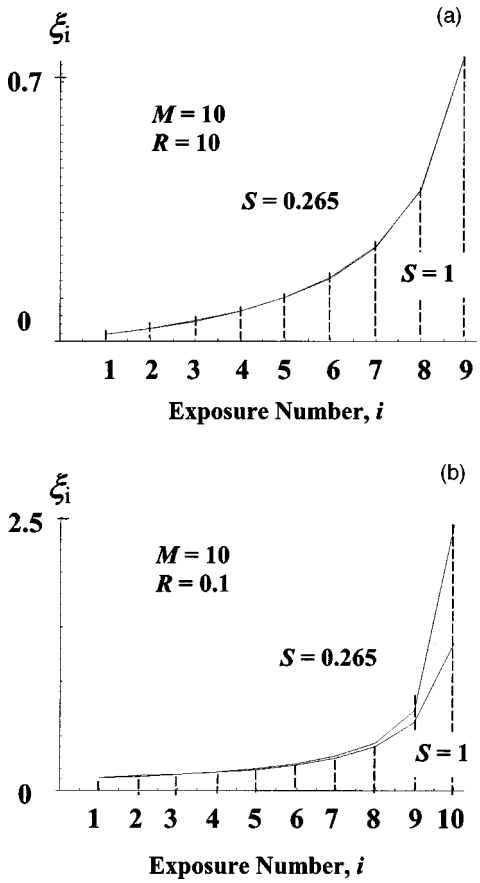

Fig. 7. (a) ξ_i plotted as a function of i for the first nine exposures. $M = 10$, $\gamma = 1/2$ (nonlinear). The almost identical $S = 0.265$ and $S = 1$ cases are shown. (b) ξ_i plotted as a function of i for all $M = 10$ exposures. $\gamma = 1/2$ (nonlinear). Both the $S = 0.265$ and $S = 1$ cases are shown.

Table 5. Corresponding to Fig. 2(a)

Local, $S = 1$; Nonlinear, $\gamma = 1/2$				
	$R = 0.1$, $\xi_M = 1.349$		$R = 10$, $\xi_M = 42.86$	
M	ξ_1	N_1	ξ_1	N_1
10	0.1004	0.05524	0.11616	0.06398
50	0.0215	0.01267	0.02223	0.01309
100	0.0109	0.00648	0.01110	0.00659
500	0.0022	0.00132	0.00220	0.00133
1000	0.0011	0.00066	0.00110	0.00067

Table 6. Corresponding to Fig. 2(b)

Nonlocal, $S = 0.265$; Nonlinear, $\gamma = 1/2$				
	$R = 0.1$, $\xi_M = 2.4388$		$R = 10$, $\xi_M = 40.211$	
M	ξ_1	N_1	ξ_1	N_1
10	0.11060	0.01653	0.11679	0.01747
50	0.02212	0.00348	0.02238	0.00351
100	0.01108	0.00180	0.01114	0.00176
500	0.00222	0.00035	0.00222	0.00035
1000	0.00111	0.00018	0.00111	0.00017

able. Practical implementations may therefore involve either leaving a significant amount of unpolymerized monomer within the material or the optimization of the recording schedule using criteria different than those proposed here.

These results also hold true when even larger numbers of gratings are recorded. In Table 3, the behavior of this local ($S = 1$) linear ($\gamma = 1$) material, when $M = 10$, 50, 100, and 1000, is presented. For each value of R the common ξ_M, and the values of ξ_1 and N_1, are given. We note that as R increases, ξ_M increases, while as M increases, ξ_1 decreases and N_1 decreases, both becoming almost identical for the two R values.

In Table 4, the analogous results for the case of $R = 0.1$ for a nonlocal ($S = 0.265$) linear material ($\gamma = 1$) are presented. The effect of introducing the nonlocality is to increase ξ_M and all the schedule values, while reducing the amplitude of each grating. To illustrate the general validity of our results, we also present results for this material when $R = 100$ and 0.01. For $R = 100$, $\xi_M = 37.1494$, and when $M = 1000$, $\xi_1 = 0.001000$ and $N_1 = 0.000264943$. When $R = 0.01$, then $\xi_M = 2.2440$, and for $M = 1000$, $\xi_1 = 0.0009997$ and $N_1 = 0.00026476$. Thus the general trends observed for $R = 0.1$ and $R = 10$ hold true.

Next, the nonlinear materials, $\gamma = 1/2$, governed by the behavior shown in Figs. 2(a) and 2(b), are examined. We graph the schedules for $M = 10$, in Fig. 7(a) for $R = 10$, and in Fig. 7(b) for $R = 0.1$. In each figure, the schedules when $S = 1$ and $S = 0.265$ are presented. In Fig. 7(a), only the first nine of the ten ξ_i values are plotted because both ξ_M values are so large (>40; see Tables 5 and 6). In Fig. 7(b), ξ_i is plotted as a function of i for all $M = 10$ exposures. Examining the results, we see that when $R = 10$, the schedules are almost identical for both S values; however, the corresponding ξ_i values are smaller than in the $R = 0.1$ case. The effect of the nonlinearity, γ, has been to decrease N_1 and slightly increase the ξ_1 value. The most significant effect of decreasing S is to decrease the grating amplitude achievable by a factor of up to 4.

Once again, to test the range of validity of these results, for the nonlocal ($S = 0.265$) nonlinear ($\gamma = 1/2$) material presented in Table 6, we examine the cases when $R = 100$ and $R = 0.01$. Setting $R = 100$, we get $\xi_M = 40.107288$, and in the case when $M = 1000$, $\xi_1 = 0.001111$ and $N_1 = 0.00017661$. Furthermore, if $R = 0.01$, then $\xi_M = 2.259032$, and for $M = 1000$, $\xi_1 = 0.001110$ and $N_1 = 0.00017646$. Once again, the trends observed for $R = 0.1$ and 10 hold true.

5. CONCLUSIONS

Using the nonlocal polymerization-driven diffusion model, NPDD, we have presented, for the first time to our knowledge, a theoretical methodology that allows an optimum recording schedule to be derived. We have explored the effects of varying M, R, γ, and S, on both the schedule and the resulting stored grating amplitudes' sizes for representative parameter values. Our methodology is based on a clear set of physical assumptions and approximations, which we have detailed and discussed.

The results of the analysis include the following:

(a) The individual ξ_i values in the exposure schedule are independent of the number of gratings to be recorded.

(b) Implementing the optimum schedule may necessitate leaving unpolymerized monomer at the end of the recording process, $u_0(\xi_M) > 0$.

(c) The effects on the schedule values, ξi, of the nonlocal response function becomes most significant as $i \rightarrow M$ and as R decreases in size. From our results, the largest percentage differences between schedules occur for $i = M$, $S = 1$, and $R = 0.1$.

(d) If a good data storage material is characterized by a low ratio between the first and last exposure, ξ_M/ξ_1, indicating a narrow range of required exposure values, then a material with a low value of R is best. We recall that a low value of R implies $F_0 > D$, and for long exposures, this indicates a lower fidelity recording material (the production of significant higher grating harmonics).

(e) If a good data storage material is primarily characterized by large uniform grating strength, then the more local the material, $S \rightarrow 1$, and the more linear the material, $\gamma \rightarrow 1$, the better the material performance.

(f) The value of R is of decreasing significance as the number of gratings recorded, M, increases. This is particularly true for the ξi values when $i < M$ and $M > 100$.

(g) Having examined the accuracy of the approximate N_1 formulas for the case of short exposures, and also for use in estimating the value of ξ_M, we conclude that more exact numerical techniques will be required to more accurately identify the optimum schedule.

Several possible extensions of both the NPDD and the schedule optimization procedure method presented here are currently being examined.[19] In the case of the NPDD, it has been assumed that a linear relationship exists between monomer concentration and the rate of polymerization.[13,14] We are currently examining this assumption motivated by the reported variation of κ as a function of ξ, which we have observed in our experimental results.[20,21] In the case of the schedule optimization algorithm, it is necessary that other optimization criteria and more general exposing intensity patterns be examined. In general, the pre-exposure encoding of data[24] may be used to improve over all holographic data storage system performance. Finally, the effects of imperfections in the recorded gratings, and thus on the readout diffraction efficiency, and the inclusion of relaxation time between exposures, must be explored as constraints on the optimization procedure.

ACKNOWLEDGMENTS

We acknowledge the support of Enterprise Ireland (Research Innovation Fund) and Science Foundation Ireland (Basic Research programme). One of the authors (F. T. O'Neill) currently holds an Irish Research Council for Engineering, Science and Technology/Embark Postdoctoral Research Fellowship.

*Corresponding author: john.sheridan@ucd.ie.

REFERENCES

1. G. Manivannan and R. A. Lessard, "Trends in holographic recording materials," Trends Polym. Sci. **2**, 282–290 (1994).
2. J. R. Lawrence, F. T. O'Neill, and J. T. Sheridan, "Photopolymer holographic recording material," Optik (Stuttgart) **112**, 449–463 (2001).
3. L. Dhar, A. Hale, H. E. Katz, L. Schilling, M. G. Schnoes, and F. C. Schilling, "Recording media that exhibit high dynamic range for digital holographic data storage," Opt. Lett. **24**, 487–489 (1999).
4. M. G. Schnoes, L. Dhar, M. L. Schilling, S. S. Patel, and P. Wiltzius, "Photopolymer-filled nanoporous glass as a dimensionally stable holographic recording medium," Opt. Lett. **24**, 658–660 (1999).
5. A. Pu and D. Psaltis, "High density recording in photopolymer-based holographic three-dimensional disks," Appl. Opt. **35**, 2389–2398 (1996).
6. L. Dhar, K. Curtis, M. Tackitt, M. Schilling, S. Campbell, W. Wilson, A. Hill, C. Boyd, N. Levinos, and A. Harris, "Holographic storage of multiple high-capacity digital data pages in thick photopolymer systems," Opt. Lett. **23**, 1710–1712 (1998).
7. R. R. A. Syms, *Practical Volume Holography* (Oxford University, Oxford, 1991).
8. S.-D. Wu and E. N. Glytsis, "Holographic grating formation in photopolymers: analysis and experimental results based on a nonlocal diffusion model and rigorous coupled-wave analysis," J. Opt. Soc. Am. B **20**, 1177–1188 (2003).
9. A. Sato, M. Scepanovic, and R. Kostuk, "Holographic edge-illuminated polymer Bragg gratings for dense wavelength division optical filters at 1550 nm," Appl. Opt. **42**, 778–784 (2003).
10. W. L. Wilson, K. R. Curtis, K. Anderson, M. C. Tackitt, A. J. Hill, M. Pane, C. Stanhope, T. Earhart, W. Loechel, C. Bergman, K. Wolfgang, C. Shuman, G. Hertrich, K. Parris, K. Malang, B. Riley, and M. Ayer, "Realization of high performance holographic data storage: The inPhase Technologies demonstration platform," Proc. SPIE **5216**, 178–191 (2003).
11. G. J. Steckman, A. Pu, and D. Psaltis, "Storage density of shift-multiplexed holographic memory," Appl. Opt. **40**, 3387–3394 (2001).
12. T. Tanaka and S. Kawata, "Comparison of recording densities in three-dimensional optical storage systems: multilayered bit recording versus angularly multiplexed holographic recording," J. Opt. Soc. Am. A **13**, 935–943 (1996).
13. J. T. Sheridan and J. R. Lawrence, "Nonlocal response diffusion model of holographic recording in photopolymer," J. Opt. Soc. Am. A **17**, 1108–1114 (2000).
14. J. R. Lawrence, F. T. O'Neill, and J. T. Sheridan, "Adjusted intensity nonlocal diffusion model of photopolymer grating formation," J. Opt. Soc. Am. B **19**, 621–629 (2002).
15. F. T. O'Neill, J. R. Lawrence, and J. T. Sheridan, "Comparison of holographic photopolymer materials using analytic nonlocal diffusion models," Appl. Opt. **41**, 845–852 (2002).
16. F. T. O'Neill, J. R. Lawrence, and J. T. Sheridan, "Comparison of holographic photopolymer materials using analytic nonlocal diffusion models: errata," Appl. Opt. **42**, 3435 (2003).
17. C. Neipp, A. Beléndez, S. Gallego, M. Ortuño, I. Pascual, and J. T. Sheridan, "Angular responses of the first and second diffracted orders in transmission diffraction grating recorded on photopolymer material," Opt. Express **11**, 1835–1855 (2003).
18. C. Neipp, A. Beléndez, J. T. Sheridan, J. V. Kelly, F. T. O'Neill, S. Gallego, M. Ortuño, and I. Pascual, "Nonlocal polymerization driven diffusion based model: general dependence of the polymerization rate to the exposure intensity," Opt. Express **11**, 1876–1886 (2003).
19. J. T. Sheridan, F. T. O'Neill, and J. V. Kelly, "Photopolymer holographic materials: the nonlocal diffusion model," in *Photorefractive Effects, Materials, and Devices*, P. Delaye,

C. Denz, L. Mager, and G. Montemezzani, eds., Vol. 87 of OSA Trends in Optics and Photonics (Optical Society of America, Washington, D.C., 2003), pp. 206–212.
20. J. V. Kelly, F. T. O'Neill, and J. T. Sheridan, "Holographic photopolymer materials with nonlocal and nonlinear response," Proc. SPIE **5216**, 127–138 (2003).
21. J. R. Lawrence, F. T. O'Neill, and J. T. Sheridan, "Photopolymer holographic recording material parameter estimation using a non-local diffusion based model," J. Appl. Phys. **90**, 3142–3148 (2001).
22. S. Piazzolla and B. K. Jenkins, "First-harmonic diffusion model for holographic grating formation in photopolymers," J. Opt. Soc. Am. B **17**, 1147–1157 (2000).
23. F. T. O'Neill, J. R. Lawrence, and J. T. Sheridan, "Improvement of holographic recording material using aerosol sealant," J. Opt. A **3**, 20–25 (2001).
24. A. Vardy, M. Blaum, P. H. Siegel, and G. T. Sincerbox, "Conservative arrays: multidimensional modulation codes for holographic recording," IEEE Trans. Inf. Theory **42**, 227–230 (1996).